Microtubule Imaging Reveals Cytoskeletal Deficit Predisposing the Retinal Ganglion Cell Axons to Atrophy in DBA/2J

Denis Sharoukhov, Festa Bucinca-Cupallari, and Hyungsik Lim

Department of Physics and Astronomy, Hunter College and the Graduate Center of the City University of New York, New York, New York, United States

Correspondence: Hyungsik Lim, Department of Physics and Astronomy, Hunter College and the Graduate Center of the City University of New York, 695 Park Avenue, 1237HN, New York, New York, 10065, USA; hyungsik.lim@hunter.cuny.edu.

Submitted: February 19, 2018
Accepted: September 4, 2018

Citation: Sharoukhov D, Bucinca-Cupallari F, Lim H. Microtubule imaging reveals cytoskeletal deficit predisposing the retinal ganglion cell axons to atrophy in DBA/2J. *Invest Ophthalmol Vis Sci*. 2018;59:5292–5300. https://doi.org/10.1167/iovs.18-24150

Purpose. Glaucoma is characterized by progressive loss of the retinal ganglion cells (RGCs) and their axons. Here we test an outstanding notion that microtubules (MTs) within RGC axons degrade before the loss of morphology ("MT hypothesis").

Methods. The integrity of axonal MTs was interrogated by intrinsic second-harmonic generation (SHG) microscopy. Using DBA/2J mice as a model of glaucoma and DBA/2J-*Gpnmb*+ as a nonglaucomatous control, the relationship between MT disruption and morphology was quantitatively examined as a function of age and sex in the fresh retinal wholemounts.

Results. The mean SHG density (i.e., the mean SHG intensity per thickness) was significantly lower in DBA/2J than in DBA/2J-*Gpnmb*+ and also depended on sex and age. The loss of SHG density, indicating MT disruption within intact RGC axons, occurred in a sectorial manner near the loss of the retinal nerve fiber bundles. The decay rate of SHG density was approximately 97% higher than that of thickness.

Conclusions. Collectively, the results indicate that the breakdown of MTs is pathology of glaucoma and likely a precursor of morphological atrophy. Based on a new finding that SHG density is highly variable and spatially discrete, a new model of RGC degeneration is proposed. This study validates SHG retinal imaging for elucidating the role and mechanism of MT deficiency in the course of glaucoma pathogenesis.

Keywords: microtubule, retinal ganglion cell, glaucoma, multiphoton microscopy

Glaucoma is the second leading cause of blindness worldwide, in which the retinal ganglion cells (RGCs) are gradually lost via apoptosis along with their axons that make up the retinal and optic nerves. Although the risk factors are known to include age and elevated IOP, their mechanistic link to RGC death is not well understood. Microtubule (MT) is a highly labile polymer whose structure is maintained by active regulation. In the context of axon, it is characterized by distinct properties that are absent in dendrites, including uniform orientation, which is crucial for axonal transport.[1,2] The stability and polarity of MTs defining the axonal identity may have significance in health and diseases. In the progression of glaucoma, the MT cytoskeleton within RGC axons has been suggested to degrade, depriving the cells of essential tropic factors.[3–6] Furthermore, the disruption of MTs has been thought to precede the loss of RGC axons ("the MT hypothesis of glaucoma").[7,8] Testing the MT hypothesis requires the integrity of axonal MTs to be measured in the fresh tissue, for which the high reflectance and birefringence of MTs have been used.[9,10] Most other techniques that have contributed substantially to our understanding of the MT dynamics in vitro or in living cells[11,12] fail to probe the native cytoskeleton in live tissue.

Here we demonstrated the use of label-free, quantitative second-harmonic generation (SHG) imaging to test the MT hypothesis. Using DBA/2J mice as an experimental model of glaucoma[13] and DBA/2J-*Gpnmb*+ mice as a nonglaucomatous control,[14] MT deficit within the RGC axons was quantitatively analyzed to compare the relative progression of the cytoskeletal integrity and morphology as a function of age.

Methods

Animals and Preparation of the Retina

The experiments were performed according to the procedures approved by Hunter College Institutional Animal Care and Use Committee and adhered to the ARVO Statement for the Use of Animals in Ophthalmic and Vision Research. DBA/2J and DBA/2J-*Gpnmb*+ mice were acquired from Jackson Laboratory (Bar Harbor, ME, USA) (#000671 and #007048) and housed in the animal facility at Hunter College.

Before imaging, animals were euthanized by CO_2 inhalation and the eye was enucleated. The retinal wholemounts were prepared and immersed into oxygenated PBS solution for imaging. It took less than 30 minutes from an animal's euthanasia to the beginning of imaging, and imaging took approximately 1.5 hours.

SHG Microscopy

The experimental setup was as described previously.[15] For exciting SHG, short pulses from a mode-locked Ti:Sapphire laser (Chameleon Ultra, Coherent, Inc.) were used. The

excitation wavelength was at 808 nm. The laser beam was focused using a water-dipping objective lens (Nikon CFI75, ×16 0.8NA; Nikon, Tokyo, Japan). The theoretical lateral and axial resolutions (i.e., the full width at half-maximum of the point spread function) were 0.37 and 1.87 μm, respectively. The polarization of the excitation beam was controlled by a polarization state generator containing two liquid crystal variable retarders (Meadowlark Optics, Inc., Frederick, CO, USA) and a quarter-wave plate (Thorlabs, Inc., Newton, NJ, USA). The average power was approximately 20 to 50 mW at the sample. SHG signal emitting from the sample was collected in the forward direction with another objective lens (Olympus UApo340, ×40 1.35NA; Olympus, Tokyo, Japan), and detected through a narrowband spectral filter of approximately 404 nm (Chroma, Taoyuan, Taiwan) and a photomultiplier tube (PMT; Hamamatsu H10492-003; Hamamatsu, Shizuoka, Japan). To cover an area of 2.5 mm^2 around the optic nerve head (ONH), z-stacks were acquired in nine regions around the ONH, including one at the ONH and eight around it along the circumference. Each had a square field of view of 650 × 650 μm. Pixel size was 1.27 μm. Z-stacks of SHG images were acquired in 2-μm axial steps. Each region was imaged twice for orthogonal linear polarizations of the excitation.

Image Corrections

Image processing was performed using Fiji/ImageJ (http://imagej.nih.gov/ij/; provided in the public domain by the National Institutes of Health, Bethesda, MD, USA).[16] The integrated SHG intensity was obtained by sum-projecting z-stack SHG images where fixed background noise was removed by subtracting the minimum-projection (Supplementary Materials, Supplementary Fig. S1). Then two images corresponding to the horizontal and vertical polarizations of excitation were summed ($I_{SHG} = I_{SHG,H} + I_{SHG,V}$). The SHG intensity can be modulated by the orientation of MTs relative to the excitation beam. To compensate for the geometrical effect, a correction factor was calculated by modeling MT as a uniaxial molecule. The integrated SHG intensity was calibrated according to the following formula (Supplementary Materials, Supplementary Fig. S2):

$$I_{SHG}(\varphi = 0) = I_{SHG}(\varphi) / \left(0.8 / \left(1 + \left(\frac{dz}{dr}\right)^2\right) + 0.2\right) \quad (1)$$

The gradient $\frac{dz}{dr}$ was evaluated from the topography of the retinal flatmount (Supplementary Materials, Supplementary Fig. S3).

Morphometry

The thickness of the retinal nerve fiber was determined by an automatic algorithm based on image segmentation for classifying the object and the background of an image. Many techniques are available for image segmentation,[17–19] including the Otsu method we used in the previous morphometry.[15,20] Because it was crucial for the outcome to be context-independent (i.e., the threshold was independent of the relative sizes of the object and the background due to axonal degeneration), the following procedure was developed involving two key steps of edge detection and histogram-based thresholding (Supplementary Materials, Supplementary Fig. S4). First, the pixels around the boundary between the nerve and background were selected, containing comparable amounts of the object and the background, so that the background did not dominate the histogram. A binary mask was created for sampling near-border pixels by detecting edges with the Sobel filter and expanding them via Gaussian blur to the width of approximately 8 pixels, which was then applied to the average-projection of z-stack images. Second, the threshold was determined by performing a variant of the triangle method[21] on the histogram of the sampled pixels. The thresholded z-stack binary images indicated whether each voxel belonged to the object (i.e., the retinal nerve fibers) or the background. Subsequently, a two-dimensional thickness map was obtained by multiplying the sum-projection of the z-stack binary images with the size of axial step (2 μm). The precision of thickness estimation was fundamentally limited by the diffraction-limited resolution of SHG microscopy and in practice could not be better than the size of axial step.

Calibration of SHG Density

The integrated SHG intensity depended on the experimental variables that are undetermined, such as the laser power on the sample, the efficiency of SHG signal collection, and the gain of PMT detector, which confounded comparing SHG intensities from different retina samples. To study the changes across the age and strain, the acquired SHG signal must be properly calibrated to eliminate the experimental variables. To address this problem, the integrated SHG intensity of each sample was normalized by the Fano factor. The underlying theory is provided from fluctuation analysis described as follows. The SHG intensity is:

$$I_{SHG}(Z) = \eta \cdot Z \cdot C_0, \quad (2)$$

where Z is the thickness of the nerve, C_0 is the concentration of MTs per unit thickness, and the proportionality coefficient η includes the effect of undetermined experimental parameters. The integrated SHG intensity can vary from pixel to pixel even for the same thickness of the retinal nerve fiber bundles in the presence of the variations of the concentration of MTs. The degree of variations is characterized by the Fano factor of the integrated SHG intensity:

$$F_I(Z) = \frac{\sigma^2_{I_{SHG}}}{\mu_{I_{SHG}}} = \eta \cdot Z \cdot \frac{\sigma^2_{C_0}}{\mu_{C_0}} = \eta \cdot Z \cdot F_{C_0}, \quad (3)$$

where μ and σ^2 denote the mean and the variance, respectively. It is noted that the Fano factor has the same dependence on the proportionality coefficient and the thickness, and also has the unit of the intensity. Thus, it can provide a reference to normalize the integrated SHG intensity across different retina samples as long as the dispersion of MTs was conserved, which would be satisfied, for instance, if MTs within each pixel are independent. The integrated SHG intensity divided by the Fano factor (i.e., the normalized SHG intensity) is a function of the concentration of MTs only (i.e., free from the effect of experimental factors):

$$\tilde{I}_{SHG} = \frac{I_{SHG}(Z)}{F_I(Z)} = \frac{C_0}{F_{C_0}} \quad (4)$$

To evaluate SHG density, the Fano factor was obtained for the population of the retinal nerve fibers with a thickness exhibiting the fewest deviations of the normalized SHG intensity among the DBA/2J-*Gpnmb*+ retinas ($Z_1 = 20$ μm; Fig. 2a). Then the SHG intensity normalized as follows was independent of the experimental parameters while retaining the same dependence on the thickness of the retinal nerve as the original integrated SHG intensity.

$$\tilde{I}_{SHG} = \frac{I_{SHG}(Z)}{F_I(Z_1)} \quad (5)$$

Then SHG density was:

Table. The Number of Animals Per Group

	DBA/2J		DBA/2J-*Gpnmb*+	
Age, mo	**Male**	**Female**	**Male**	**Female**
5	1	1	0	0
6	2	1	2	0
7	1	3	1	1
8	3	5	2	1
9	4	6	1	1
10	5	4	1	1
11	4	5	0	1
12	0	5	0	3
13	0	0	0	0
14	1	1	1	0
15	0	0	1	0
Total	21	31	9	8
	52		17	

$$\rho = \frac{\tilde{I}_{SHG}}{Z} = \frac{I_{SHG}(Z)}{F_I(Z_1)}\frac{1}{Z} = \frac{\eta \cdot Z \cdot C_0}{\eta \cdot Z_1 \cdot F_{C_0}}\frac{1}{Z} = \frac{C_0}{Z_1 \cdot F_{C_0}}, \quad (6)$$

providing a measure of the concentration of MTs per unit thickness (per pixel) without the effect of experimental variables. Finally, the absolute range of SHG density was chosen such that the mean value was unity for the population of DBA/2J-*Gpnmb*+ retinas:

$$\rho = \left(\frac{C_0}{F_{C_0}}\right) / \left(\frac{C_0}{F_{C_0}}\right)_{Gpnmb+} \quad (7)$$

As a result, SHG density depended on the concentration of MTs per unit thickness (per pixel) but not on experimental variables.

Statistics

Statistical analysis was performed using R software package (http://www.R-project.org, available in the public domain).

Results

Sectorial Degeneration of RGC Axons Measured by SHG

SHG arises from uniformly polarized MT cytoskeleton in axons.[15,20,22,23] First, it was tested for confirming the known characteristic pathologies of DBA/2 mouse, including progressive and sectorial degeneration of the retinal nerve fiber bundles.[13,24–27] The retinas of DBA/2J and DBA/2J-*Gpnmb*+ mice (n = 52 and 17, respectively) were imaged by SHG microscopy at ages from 5 to 16 months (Table). Figure 1a depicts representative mosaics created from the average projections of z-stack SHG images. The retinal nerve fiber bundles in DBA/2J mice were gradually lost at ages of >9 months, whereas no sign of degeneration was observed in DBA/2J-*Gpnmb*+ mice at all ages we examined. The arteries and veins were also visualized due to SHG stemming from collagenous tissues, which did not degrade with age. The total volume of the retinal nerve fiber bundles could be evaluated for quantitative analysis. As expected, it decreased with age in DBA/2J mice, whereas it was relatively conserved in DBA/2J-*Gpnmb*+ mice (Fig. 1b). The tissue volume was highly variable in older DBA/2J mice and approximately 15% persisted, which was due to the blood vessels. Furthermore, degenerating RGC axons in DBA/2J mice were occasionally found in discrete angular patches (Figs. 1c, 1d), consistent with the sectorial degeneration of RGC axons that has been observed previously by immunohistochemistry and interpreted to suggest possible mechanisms of glaucoma pathogenesis.[24–30]

MTs Lost Within Intact Axons

There are two possible scenarios for the loss of SHG signal in old DBA/2J mice; either axonal MTs were disrupted while the RGC morphology was intact, or they were compromised concurrently. The MT hypothesis predicts the former. To test this, we examined the relative magnitudes of morphology and MT integrity of the RGC axons, which could be simultaneously determined in a single SHG measurement. By virtue of the depth-sectioning capability and the sensitivity to the organization of MT cytoskeleton, SHG allowed the thickness and the MT content of the retinal nerve fiber bundles to be analyzed pixel by pixel with micrometer resolutions. We achieved objective quantification of the volume of the retinal nerve fiber bundles by SHG morphometry. With automatic image segmentation[15] providing a threshold independent of the context of image, the evaluated tissue volume was bias-free and comparable across the age.

Interestingly, there were angular regions where the SHG signal diminished considerably while the thickness was relatively normal (Fig. 1e, magenta arrows), suggesting MT deficit (i.e., low MTs within intact RGC axons). The integrity of the MT cytoskeleton is a necessary condition for SHG signals, as previously verified with pharmacological experiments.[15,22] Provided that the density of MTs was constant and homogeneous across the depth of the retinal nerve fiber bundles, SHG intensity integrated over the depth would be linearly proportional to the thickness of the retinal nerve fiber bundles. The result suggested that the amount of MT was significantly less for the thickness (i.e., the RGC axons persisted after the loss of MTs, as predicted by the MT hypothesis). Moreover, the areas of MT deficit were observed in the same retina exhibiting the sectorial loss of RGC axons.

Studying the Relationship Between Cytoskeletal Integrity and Morphology

We sought to investigate quantitatively the decoupling of MT integrity from morphology. In order for this, first the Fano factor needed to be validated as a reference of calibration. We examined whether the normalized SHG intensity is independent of the thickness, as predicted by Equation 4. Figure 2a depicts the average of normalized SHG intensity versus thickness for 17 DBA/2J-*Gpnmb*+ mice. It was relatively constant for the thick nerve fiber bundles (>10 μm) despite some deviations for the population with less than 10-μm thickness. Remarkably, the animal-to-animal deviations were modest (the coefficient of variation of approximately 0.2), indicating that the effect of experimental factors varying day-to-day was small. The method of calibration was further validated by the fact that the mean MT densities of DBA/2J-*Gpnmb*+ mice were relatively constant. Next, to unravel the relationship within the individual retina, we compared the SHG intensity summed over the axial sections and the thickness of the nerve fiber bundles. Figures 2b and 2c depict representative data of DBA/2J and DBA/2J-*Gpnmb*+, 9 and 12 months old, respectively. Overall, the SHG intensity and thickness of DBA/2J were significantly lower than those of DBA/2J-*Gpnmb*+ mice. Despite large variations, presumably stemming from the MT content weakly correlated with the thickness, the integrated SHG intensity was roughly proportional to the thickness (Pearson $r = 0.68$, $P < 0.01$ and 0.75, P

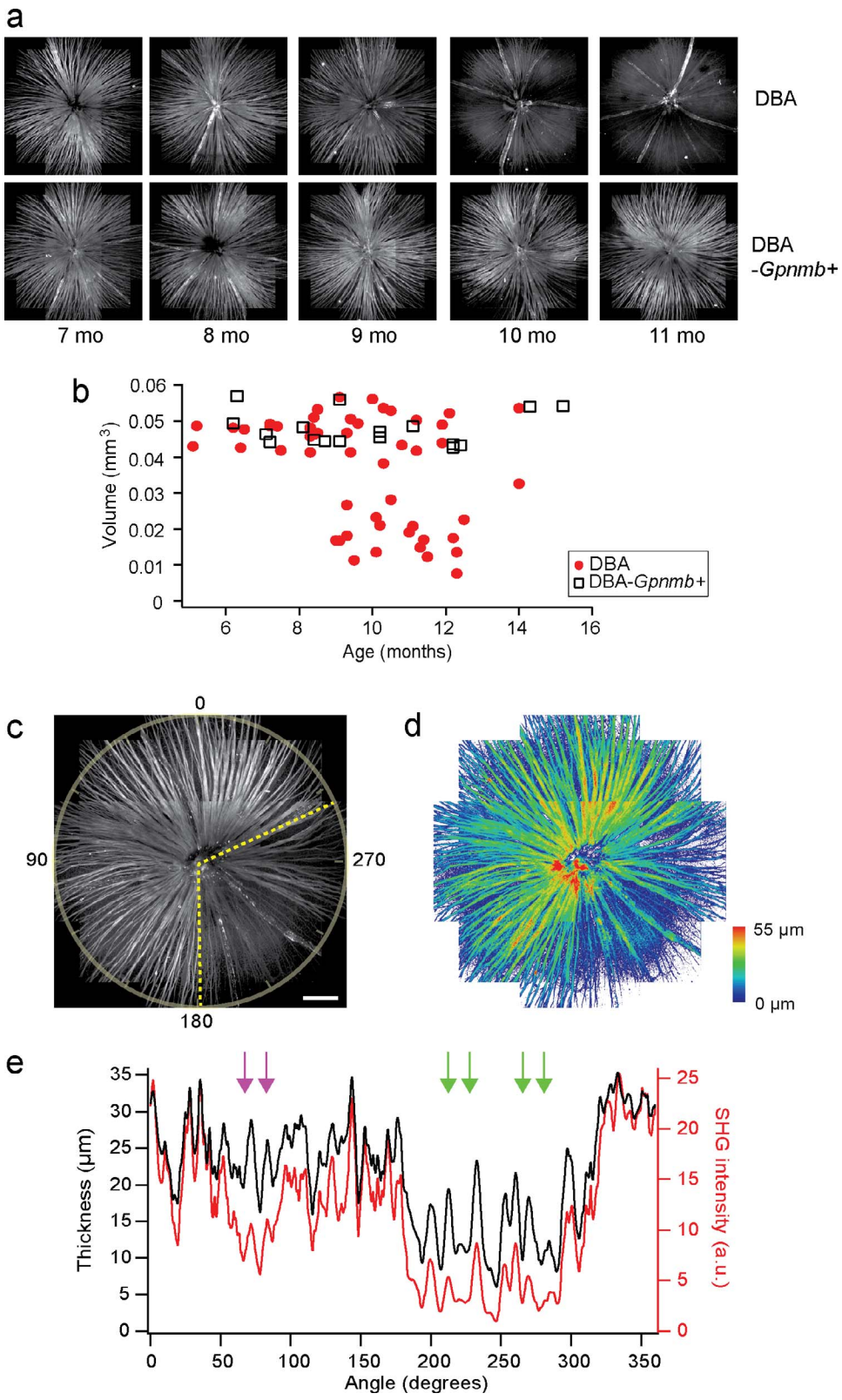

Figure 1. DBA/2J pathologies are detected by SHG imaging. (**a**) Mosaics of DBA/2J and DBA/2J-*Gpnmb*+ retinas ex vivo at ages between 7 and 11 months, showing age-dependent loss of the retinal nerve fibers only in DBA/2J mice. (**b**) The volume of the retinal nerve fibers, displaying significant decrease in DBA/2J mice older than approximately 9 months. (**c**, **d**) The integrated SHG intensity and the thickness of the DBA/2J retina (9 months old), respectively. Sectorial degeneration is delineated with *yellow dashed lines*. *Scale bar*: 200 µm. (**e**) The integrated SHG intensity and the thickness versus angle (*red* and *black*, respectively), where the regions of decoupling are marked with *arrows*. The region with low SHG but normal thickness is indicated with *magenta arrows*.

Investigative Ophthalmology & Visual Science

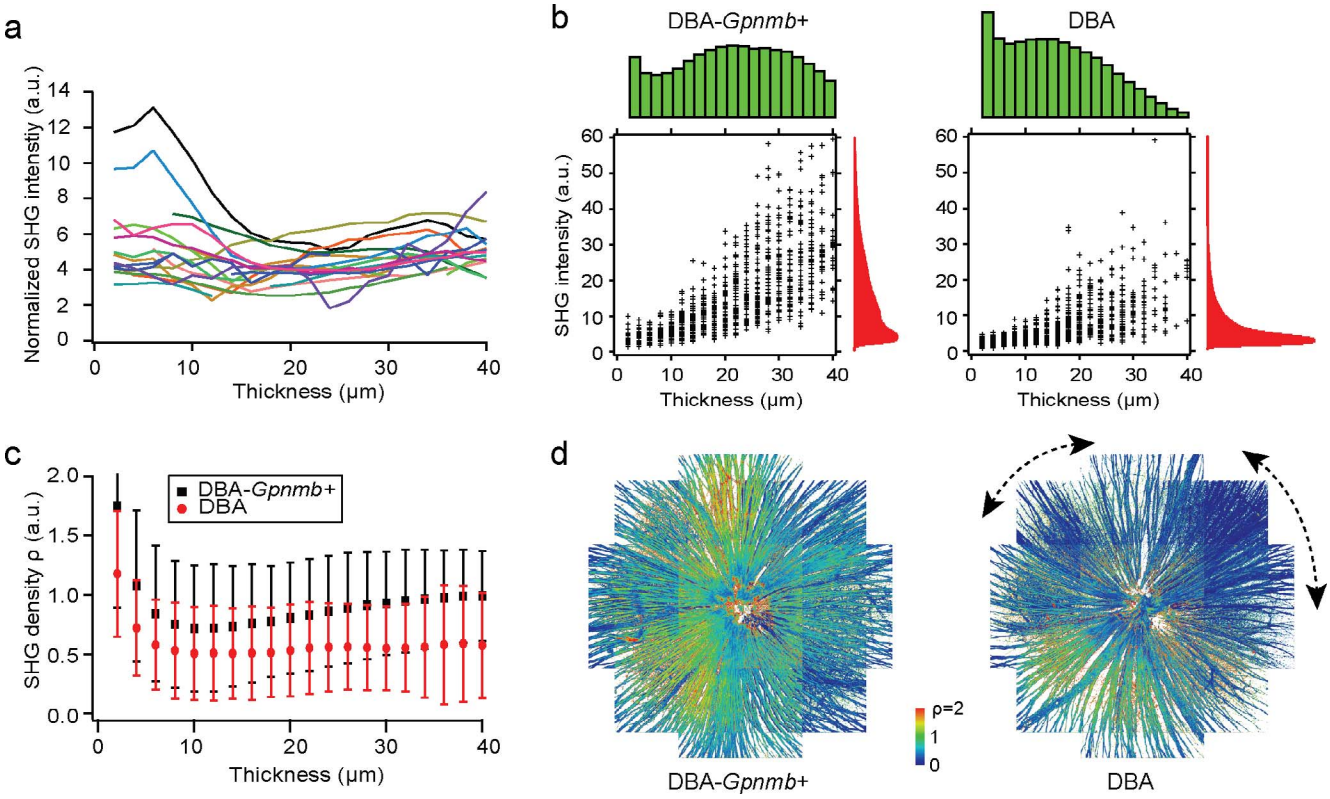

Figure 2. The relationship between axonal MT cytoskeleton and morphology. (**a**) The average normalized SHG intensity as a function of thickness (Equation 4) for DBA/2J-*Gpnmb*+ mice ($n = 17$, color-coded). (**b**) The distributions of the integrated SHG intensity (*red*) and thickness (*green*) in the retinas of DBA/2J-*Gpnmb*+ (12 months old) and DBA/2J (9 months old) mice, where scatterplots show the pixel values at randomly sampled positions ($n = 1000$). (**c**) SHG density ρ as a function of thickness of the retinal nerve fibers. (**d**) SHG density across the retinas. Angular segments of significant MT deficit within the DBA/2J retina are indicated with *dashed lines*.

< 0.01 for DBA/2J and DBA/2J-*Gpnmb*+, respectively). It seemed that the ratio of SHG intensity to the thickness, which we defined as "SHG density," can provide a surrogate measure for the quantity of MTs per unit volume. Then the decrease in SHG density would indicate decoupling between MT integrity and morphology of the RGC axons (i.e., MT deficit). By contrast, the case in which they were lost altogether was distinguishable by the reduced thickness. We found SHG density was significantly lower in the DBA/2J mice >8 months of age than in DBA/2J-*Gpnmb*+ mice. Figure 2c illustrates SHG density as a function of thickness for the representative DBA/2J and DBA/2J-*Gpnmb*+ mice. It was relatively uniform in the thick retinal nerve fiber bundles but increased below 10-μm thickness. A large fraction of the features with thickness below 10 μm could be distinguished from the retinal nerve fiber bundles, laterally as well as axially. They were presumed to belong to the axons of non-RGCs, but further identification is beyond the scope of the current study. For this work, we limited the population of SHG pixels with >10-μm thickness so that our quantitative analysis was specific to the RGCs.

Sectorial Pattern of Decreasing SHG Density

To study how SHG density was distributed across the normal retinas and whether pathological MT deficit emerged focally, we examined the SHG densities across DBA/2J and DBA/2J-*Gpnmb*+ retinas. There were topographically nonuniform distributions in both strains (Fig. 2d). The DBA/2J retina had angular segments of low SHG densities exceeding the normal range of variations (Fig. 2d, dashed lines) with no apparent correlation between the position of sectors and vasculature. The spatial distribution of MT deficit was analogous to sectorial patterns known to appear in the strain for the loss of RGC axons, soma, and also transport deficit,[24–30] which have been interpreted to suggest the ONH as the site of injury. SHG density lost in a similar fashion as other DBA/2J pathologies could likewise shed insights into the mechanism of pathogenesis. Interestingly, sectorial MT deficits, although substantially more modest in the magnitude, were also present in the normal retinas of DBA/2J-*Gpnmb*+ mice.

Age- and Sex-Dependent Loss of SHG Density

SHG density was statistically analyzed for the whole retina. Due to the significant variability of SHG intensity for the same thickness, it was confounded to determine unequivocally whether MT deficit at a particular point in the retina was pathological; however, such a characterization was nonetheless possible via statistical analysis of SHG density for the whole retina. To study how MT deficit evolved with age, we evaluated the distribution of SHG density for DBA/2J and DBA/2J-*Gpnmb*+ mice ($n = 52$ and 17, respectively). Figure 3a shows the normalized distribution (i.e., the probability density function) of five representative DBA/2J retinas at ages from 7 to 11 months (red), overlaid with the average probability density function of DBA/2J-*Gpnmb*+ retinas between ages 5 and 16 months (black). SHG density exhibited substantial animal-to-animal variations, similar to other characteristics of this strain,[31] and the normal (i.e., physiological) range of variability was specified by the average distribution of DBA/2J-*Gpnmb*+ mice. The difference between DBA/2J and DBA/2J-*Gpnmb*+ was nonetheless evident where MT densities of older

Investigative Ophthalmology & Visual Science

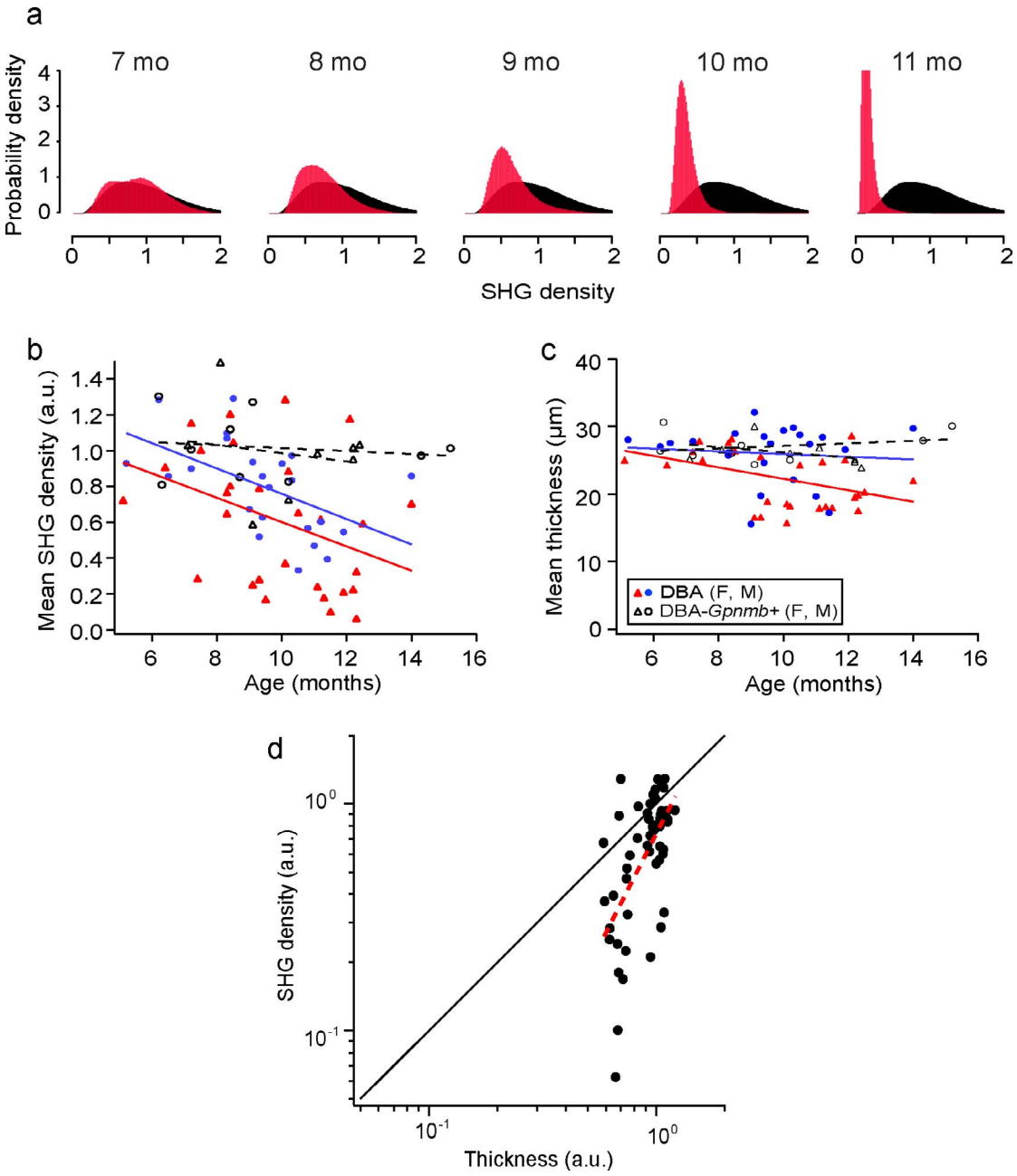

Figure 3. MT deficiency is specific to the DBA/2J strain and depends on age and sex. (**a**) The probability density functions of SHG density for DBA/2J mice at ages from 7 to 11 months (*red*), overlaid with the average of DBA/2J-*Gpnmb*+ mice between 6 and 13 months of age ($n = 17$, *black*). (**b**, **c**) The mean thickness and SHG density for DBA/2J (*red* and *blue*) and DBA/2J-*Gpnmb*+ mice (*black*) as a function of age. Two symbols (*triangle* and *circle*) denote sexes and the *dashed lines* show the linear regression. (**d**) The relative magnitudes of SHG density versus thickness of the DBA retinas across ages. The mean SHG density and the normalized mean thickness are shown on the logarithmic scales with the best fit to the model (*red dashed line*, $\alpha/\beta = 1.97$).

DBA/2J animals decreased below the normal range. The reduction in the mean SHG density, which we referred to as MT deficiency, was significant in DBA/2J at >9 months, but absent in DBA/2J-*Gpnmb*+ mice at all ages (Fig. 3b). As opposed to MT deficit, which is focal and found also in DBA/2J-*Gpnmb*+, MT deficiency was specific to the DBA/2J strain and increased with age, suggesting a phenotype associated with glaucomatous progression. It has been known that some pathological phenotypes of DBA/2J are sex-dependent.[31] To examine whether the loss of SHG density and morphology also varied depending on the sex, we used a linear regression model with interaction between age and sex. SHG density and thickness exhibited significant sex difference ($P = 0.07$ and 0.004, respectively), but their rates of decay did not ($P = 0.93$ and 0.27, respectively).

Relative Decay Rates of SHG Density and Morphology of RGC Axons

Given their outstanding similarities (i.e., DBA/2J-specific, retinotopic, and progressive with age), it is interesting to ask the relationship between MT deficiency and axonal loss. Importantly, the mean SHG density decreased more rapidly

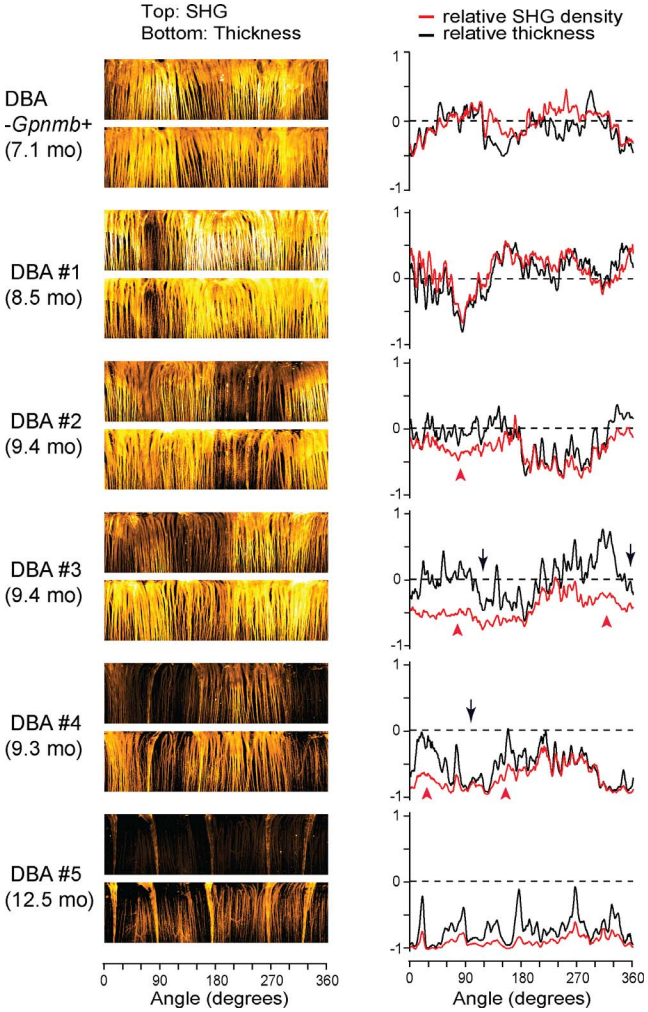

Figure 4. MT disruption and loss of RGC axons are spatially correlated. Five representative DBA/2J retinas with sectorial degeneration are depicted (#2 is the same retina as in Fig. 1e), along with one DBA/2J-*Gpnmb*+. *Left*: The integrated SHG intensity and the thickness in the polar coordinates. *Right*: The relative SHG density and the relative thickness as a function of angle. The zero lines (*dashed*) indicate the average of DBA/2J-*Gpnmb*+ ($n = 17$). The regions with significant spreads between SHG density and thickness (*red arrowheads*) are found near axonal degeneration (*black arrows*).

than the mean thickness of RGC axons for DBA/2J mice (Fig. 3c). To understand the pathogenic process quantitatively, a basic model was used in which the MT loss and axon loss initiate at the same time. Also, the rate coefficients of SHG loss (without morphological loss) and morphological loss (with collateral SHG loss) per unit volume are independent and given by α and β, respectively. Then the rate equation for the integrated SHG intensity and thickness is:

$$\frac{dI}{dt} = -(\alpha + \beta) \cdot I, \quad \frac{dZ}{dt} = -\beta \cdot Z. \tag{8}$$

For the SHG density:

$$\frac{d\rho}{dt} = \frac{d\left(\frac{I}{Z}\right)}{dt} = -\alpha \cdot \rho. \tag{9}$$

Consequently, the rate coefficients can be determined separately from SHG density and thickness. We sought to determine the relative rates, which can be done more accurately by following the relative magnitudes of SHG density and thickness in the same animals:

$$\frac{d\rho}{dZ} = \frac{d\rho/dt}{dZ/dt} = \frac{\alpha}{\beta} \cdot \frac{\rho}{Z}, \quad \rho = \left(\frac{Z}{Z_0}\right)^{\frac{\alpha}{\beta}}. \tag{10}$$

We studied the mean SHG density versus the mean thickness on the logarithmic scales (Fig. 3d). The best fit to the measured data (red dashed line) yielded the ratio of rate coefficients α/β of approximately 1.97 ± 0.39 (i.e., the decay rate of SHG density was approximately 97% higher than that of morphological loss); however, this simple model did not account for the possibility that the rate coefficients may change over time $\alpha = \alpha(t), \beta = \beta(t)$. If the loss of RGC axons is delayed relative to the loss of MTs, for instance, this can result in larger deviations between SHG density and thickness (i.e., farther from the diagonal line in Fig. 3d), as we observed within the single DBA/2J retinas (Fig. 4).

Spatial Correlation Between Loss of SHG Density and Loss of RGC Axons

We investigated if there was any spatial relationship between the loss of RGC axons and SHG density by comparing in the same DBA/2J retinas. Five representative DBA/2J samples and one DBA/2J-*Gpnmb*+ are depicted with the SHG intensity and the thickness in the polar coordinates (Fig. 4, left panels). There were dark areas in the SHG and thickness maps, respectively, indicating the sectorial degradation of MTs and the RGC axons. There were also regions of substantial MT deficit, where SHG intensity was lost but not the morphology, similar to the decoupling in Figure 1e. To unravel the spatial relationship, we evaluated the relative SHG density (ρ-1) and the relative thickness ($Z/Z_0 - 1$, where Z_0 is the average thickness of DBA/2J-*Gpnmb*+ retinas) (Fig. 4, right), where the zero baselines denoted the average values of the DBA/2J-*Gpnmb*+. Then the regions with wide spreads between SHG density and thickness revealed the areas of pathological MT deficit (red arrowheads). Interestingly, they were frequently found in close proximity to moderate axonal degeneration (black arrows). The spatial correlation between the pathological MT deficit and loss of RGC axons may shed light into the mechanism of MT deficiency.

Discussion

We have demonstrated MT deficiency as a novel endogenous glaucoma marker. Using the DBA/2J mouse model and SHG imaging, we have presented a support for the MT hypothesis (i.e., MT cytoskeleton is disrupted before the loss of RGC axons in the course of glaucomatous progression). The loss of axonal MTs is associated with disease pathogenesis, being DBA/2J-specific and initiates at an age that roughly coincides with the onset of IOP elevation.[31] Moreover, the spatiotemporal relationship of MT deficiency and axonal atrophy supports the notion that cytoskeletal breakdown predisposes the RGC axons to degeneration. The distribution of MT-compromised RGC axons is topologically discrete, analogous to the sectorial degeneration of RGCs observed previously in various models of experimental glaucoma[32] as well as human disease.[33] Similar to the spatial pattern of axonal degeneration, which suggests possible causes of glaucoma at the ONH, the spatial profile of MT loss can provide an insight into the pathogenic mechanism. In particular, MT-compromised RGC axons are routinely found near degenerating axons, leading to a speculation about a common cause underlying MT disruption and axonal loss (e.g., mechanical insults at the ONH) as well as temporal causation

in the course of RGC degeneration.[34,35] Remarkably, the relative magnitude of the loss of SHG density to the loss of morphology becomes more significant with ages. Taken together, these results suggest that MT disruption is pathology of glaucoma. It follows that MT deficiency may be present also in other models of experimental glaucoma as well as human disease, which should be verified in future studies. Determining the relative course of MT deficiency and other features of RGC degeneration would be significant not only for earlier detection and treatment of glaucoma but can also elucidate the mechanism of glaucoma pathogenesis. Also, it is crucial to determine whether MT deficiency is a general rule of axonal degeneration or specific to glaucomatous progression.

The observed variability of MT deficit permits a new model of RGC pathogenesis, in which the breakdown of MTs is hypothesized as an element of the axonal self-destruction. Glaucoma has been considered as primarily a disease of axons where the RGC is a compartmentalized unit with the soma and axon undergoing independent pathways of self-destruction.[36–38] The axonal self-destruction exhibits various cell-autonomous characteristics.[39] It is possible that MT deficiency plays an active role in the self-destruction program, or is a downstream effect associated with the apoptotic pathways. It is interesting that SHG density has such significant variations within the individual retina (Fig. 2a), whereas the mean level is relatively conserved across the normal population (Fig. 4b). Considering that the amount of MTs is regulated in proportion to the axon diameter through complex mechanisms involving microtubule-associated proteins (MAPs)[40] and other cytoskeletal proteins,[41–43] a question can be raised regarding the molecular basis of highly variable SHG density (e.g., permissive regulations). More importantly, substantial MT deficit can be postulated as providing a molecular substrate for the susceptibility of RGC axons to IOP. The fact that elevated IOP is neither necessary nor sufficient for developing glaucoma has led some to argue that the sensitivity of the RGCs to elevated IOP, rather than the magnitude of IOP, is more pertinent to triggering the pathogenic pathway.[35] Because the MT network is responsible for a significant portion of the axon's mechanical property, it is conceivable that lower SHG density renders RGC axons more vulnerable to elevated IOP. For example, we have found that even the healthy retinas exhibit isolated regions with lower SHG density (Fig. 2d). The hypothesis predicts that they are the loci whereupon IOP-induced injury to the self-destruction pathway initiates, eventually causing sectorial loss of RGC axons.

SHG retinal imaging has been validated by this study where the use of SHG was crucial as a surrogate to measure MT deficiency for illuminating the relationship with morphology. To date, this subject has been studied primarily by measuring the reflectance or birefringence of MTs because most other imaging techniques are not adequate for probing MTs in living tissue. Unlike immunohistochemistry or fluorescent protein, which tags to tubulins regardless of MT conformation,[44] SHG does not arise from depolymerized tubulins or chemically crosslinked MTs, and hence is absent from degenerating cells in which MT assembly is thermodynamically unstable and gradually dissociates without active regulation. SHG is emitted only from the functionally active form of MTs (i.e., uniformly polarized MTs found in axons[1]), which is required for axonal transport. The failure of axonal transport has been measured using a variety of tracers, but the lack of the tracer signals can be attributed to diverse factors, such as ATP hydrolysis and motor proteins, not just MT cytoskeleton. By contrast, loss of SHG would be specifically due to the disruption of MT cytoskeleton in the RGC axons. Consequently, the demonstrated SHG technique should be useful to determine the relative progression of axonal MT disruption and other emerging molecules of pathogenesis.[45]

Acknowledgments

Supported by funding from the BrightFocus Foundation (G2013143) and the National Institutes of Health (GM121198).

Disclosure: **D. Sharoukhov**, None; **F. Bucinca-Cupallari**, None; **H. Lim**, None

References

1. Baas PW, Deitch JS, Black MM, Banker GA. Polarity orientation of microtubules in hippocampal neurons—uniformity in the axon and nonuniformity in the dendrite. *Proc Natl Acad Sci U S A*. 1988;85:8335–8339.
2. Baas PW, Mozgova OI. A Novel role for retrograde transport of microtubules in the axon. *Cytoskeleton*. 2012;69:416–425.
3. Balaratnasingam C, Morgan WH, Bass L, Matich G, Cringle SJ, Yu DY. Axonal transport and cytoskeletal changes in the laminar regions after elevated intraocular pressure. *Invest Ophthalmol Vis Sci*. 2007;48:3632–3644.
4. Balaratnasingam C, Morgan WH, Bass L, Cringle SJ, Yu DY. Time-dependent effects of elevated intraocular pressure on optic nerve head axonal transport and cytoskeleton proteins. *Invest Ophthalmol Vis Sci*. 2008;49:986–999.
5. Fortune B, Burgoyne CF, Cull GA, Reynaud J, Wang L. Structural and functional abnormalities ofretinal ganglion cells measured in vivo at the onset of optic nerve head surface change in experimental glaucoma. *Invest Ophthalmol Vis Sci*. 2012;53:3939–3950.
6. Fortune B, Burgoyne CF, Cull G, Reynaud J, Wang L. Onset and progression of peripapillary retinal nerve fiber layer (RNFL) retardance changes occur earlier than RNFL thickness changes in experimental glaucoma. *Invest Ophthalmol Vis Sci*. 2013;54:5653–5660.
7. Huang XR, Knighton RW. Microtubules contribute to the birefringence of the retinal nerve fiber layer. *Invest Ophthalmol Vis Sci*. 2005;46:4588–4593.
8. Huang XR, Knighton RW, Cavuoto LN. Microtubule contribution to the reflectance of the retinal nerve fiber layer. *Invest Ophthalmol Vis Sci*. 2006;47:5363–5367.
9. Huang XR, Knighton RW, Spector YZ, Qiao JZ, Kong W, Zhao Q. Reflectance spectrum and birefringence of the retinal nerve fiber layer with hypertensive damage of axonal cytoskeleton. *Invest Ophthalmol Vis Sci*. 2017;58:2118–2129.
10. Huang XR, Knighton RW, Spector YZ, Feuer WJ. Cytoskeletal alteration and change of retinal nerve fiber layer birefringence in hypertensive retina. *Curr Eye Res*. 2017;42:936–947.
11. Waterman-Storer CM, Desai A, Bulinski JC, Salmon ED. Fluorescent speckle microscopy, a method to visualize the dynamics of protein assemblies in living cells. *Curr Biol*. 1998;8:1227–1230.
12. Honnappa S, Gouveia SM, Weisbrich A, et al. An EB1-binding motif acts as a microtubule tip localization signal. *Cell*. 2009; 138:366–376.
13. John SWM, Smith RS, Savinova OV, et al. Essential iris atrophy, pigment dispersion, and glaucoma in DBA/2J mice. *Invest Ophthalmol Vis Sci*. 1998;39:951–962.
14. Howell GR, Libby RT, Marchant JK, et al. Absence of glaucoma in DBA/2J mice homozygous for wild-type versions of Gpnmb and Tyrp1. *BMC Genet*. 2007;8:45.
15. Lim H, Danias J. Label-free morphometry of retinal nerve fiber bundles by second-harmonic-generation microscopy. *Opt Lett*. 2012;37:2316–2318.
16. Schindelin J, Arganda-Carreras I, Frise E, et al. Fiji: an open-source platform for biological-image analysis. *Nat Methods*. 2012;9:676–682.
17. Weszka JS, Rosenfeld A. Histogram modification for threshold selection. *IEEE Trans Syst Man Cybern*. 1979;9:38–52.

18. Sahoo PK, Soltani S, Wong AKC, Chen YC. A survey of thresholding techniques. *Comput Vis Graph Image Process*. 1988;41:233–260.
19. Lee SU, Chung SY, Park RH. A comparative perfornace study of several global thresholding techniques for segmentation. *Comput Vis Graph Image Process*. 1990;52:171–190.
20. Lim H, Danias J. Effect of axonal micro-tubules on the morphology of retinal nerve fibers studied by second-harmonic generation. *J Biomed Opt*. 2012;17:110502.
21. Zack GW, Rogers WE, Latt SA. Automatic measurement of sister chromatid exchange frequency. *J Histochem Cytochem*. 1977;25:741–753.
22. Dombeck D, Kasischke K, Vishwasrao H, Ingelsson M, Hyman B, Webb W. Uniform polarity microtubule assemblies imaged in native brain tissue by second-harmonic generation microscopy. *Proc Natl Acad Sci U S A*. 2003;100:7081–7086.
23. Kwan AC, Dombeck DA, Webb WW. Polarized microtubule arrays in apical dendrites and axons. *Proc Natl Acad Sci U S A*. 2008;105:11370–11375.
24. Danias J, Lee KC, Zamora MF, et al. Quantitative analysis of retinal ganglion cell (RGC) loss in aging DBA/2NNia glaucomatous mice: comparison with RGC loss in aging C57/BL6 mice. *Invest Ophthalmol Vis Sci*. 2003;44:5151–5162.
25. Jakobs TC, Libby RT, Ben YX, John SWM, Masland RH. Retinal ganglion cell degeneration is topological but not cell type specific in DBA/2J mice. *J Cell Biol*. 2005;171:313–325.
26. Filippopoulos T, Danias J, Chen B, Podos SM, Mittag TW. Topographic and morphologic analyses of retinal ganglion cell loss in old DBA/2NNia mice. *Invest Ophthalmol Vis Sci*. 2006;47:1968–1974.
27. Soto I, Oglesby E, Buckingham BP, et al. Retinal ganglion cells downregulate gene expression and lose their axons within the optic nerve head in a mouse glaucoma model. *J Neurosci*. 2008;28:548–561.
28. Schlamp CL, Li Y, Dietz JA, Janssen KT, Nickells RW. Progressive ganglion cell loss and optic nerve degeneration in DBA/2J mice is variable and asymmetric. *BMC Neurosci*. 2006;7:66.
29. Howell GR, Libby RT, Jakobs TC, et al. Axons of retinal ganglion cells are insulted in the optic nerve early in DBA/2J glaucoma. *J Cell Biol*. 2007;179:1523–1537.
30. Buckingham BP, Inman DM, Lambert W, et al. Progressive ganglion cell degeneration precedes neuronal loss in a mouse model of glaucoma. *J Neurosci*. 2008;28:2735–2744.
31. Libby RT, Anderson MG, Pang IH, et al. Inherited glaucoma in DBA/2J mice: pertinent disease features for studying the neurodegeneration. *Vis Neurosci*. 2005;22:637–648.
32. Soto I, Pease ME, Son JL, Shi XH, Quigley HA, Marsh-Armstrong N. Retinal ganglion cell loss in a rat ocular hypertension model is sectorial and involves early optic nerve axon loss. *Invest Ophthalmol Vis Sci*. 2011;52:434–441.
33. Quigley HA, Addicks EM. Regional differences in the structure of the lamina cribrosa and their relation to glaucomatous optic nerve damage. *Arch Ophthalmol*. 1981;99:137–143.
34. Nickells RW. From ocular hypertension to ganglion cell death: a theoretical sequence of events leading to glaucoma. *Can J Ophthalmol*. 2007;42:278–287.
35. Calkins DJ. Critical pathogenic events underlying progression of neurodegeneration in glaucoma. *Prog Retin Eye Res*. 2012;31:702–719.
36. Whitmore AV, Libby RT, John SWM. Glaucoma: thinking in new ways—a role for autonomous axonal self-destruction and other compartmentalised processes? *Prog Retin Eye Res*. 2005;24:639–662.
37. Nickells RW, Howell GR, Soto I, John SWM. Under pressure: cellular and molecular responses during glaucoma, a common neurodegeneration with axonopathy. *Annu Rev Neurosci*. 2012;35:153–179.
38. Calkins DJ, Horner PJ. The cell and molecular biology of glaucoma: axonopathy and the brain. *Invest Ophthalmol Vis Sci*. 2012;53:2482–2484.
39. Crish SD, Sappington RM, Inman DM, Horner PJ, Calkins DJ. Distal axonopathy with structural persistence in glaucomatous neurodegeneration. *Proc Natl Acad Sci U S A*. 2010;107:5196–5201.
40. Hirokawa N. Microtubule organization and dynamics dependent on microtubule-associated proteins. *Curr Opin Cell Biol*. 1994;6:74–81.
41. Xu ZS, Marszalek JR, Lee MK, et al. Subunit composition of neurofilaments specifies axonal diameter. *J Cell Biol*. 1996;133:1061–1069.
42. Hammarlund M, Jorgensen EM, Bastiani MJ. Axons break in animals lacking beta-spectrin. *J Cell Biol*. 2007;176:269–275.
43. Xu K, Zhong GS, Zhuang XW. Actin, spectrin, and associated proteins form a periodic cytoskeletal structure in axons. *Science*. 2013;339:452–456.
44. Wilson GN, Smith M, Inman DM, Dengler-Crish CM, Crish SD. Early cytoskeletal protein modifications precede overt structural degeneration in the DBA/2J mouse model of glaucoma. *Front Neurosci*. 2016;10:494.
45. Tamm ER, Ethier CR; Lasker/IRRF Initiative on Astrocytes and Glaucomatous Neurodegeneration Participants. Biological aspects of axonal damage in glaucoma: a brief review. *Exp Eye Res*. 2017;157:5–12.

Investigative Ophthalmology & Visual Science